Received: 27 April 2023 | Accepted: 2 August 2023

DOI: 10.1097/HC9.0000000000000330

ORIGINAL ARTICLE

OPEN

Myeloid spatial and transcriptional molecular signature of ischemia-reperfusion injury in human liver transplantation

Rebecca A. Sosa[1,2] | **Richard Ahn**[3,4] | **Fang Li**[1] | **Allyson Q. Terry**[1] | **Zach Qian**[3] | **Adil Bhat**[1] | **Subha Sen**[1] | **Bita V. Naini**[1] | **Takahiro Ito**[5] | **Fady M. Kaldas**[5] | **Alexander Hoffmann**[3,4] | **Ronald W. Busuttil**[5] | **Jerzy W. Kupiec-Weglinski**[1,5] | **David W. Gjertson**[1,2] | **Elaine F. Reed**[1,2]

[1]Department of Pathology and Laboratory Medicine, UCLA, Los Angeles, California, USA

[2]Department of Pathology and Laboratory Medicine, UCLA Immunogenetics Center, UCLA, Los Angeles, California, USA

[3]Institute for Quantitative and Computational Biosciences, UCLA, Los Angeles, California, USA

[4]Department of Microbiology, Immunology, and Molecular Genetics, UCLA, Los Angeles, California, USA

[5]Department of Surgery, UCLA, Los Angeles, California, USA

Correspondence
Elaine F. Reed, Department of Pathology and Laboratory Medicine, UCLA Immunogenetics Center, UCLA, 1000 Veteran Ave. Los Angeles, CA 90095, USA.
Email: ereed@mednet.ucla.edu

Abstract

Background: Ischemia-reperfusion injury (IRI) is a significant clinical concern in liver transplantation, with a key influence on short-term and long-term allograft and patient survival. Myeloid cells trigger and sustain tissue inflammation and damage associated with IRI, but the mechanisms regulating these activities are unknown. To address this, we investigated the molecular characteristics of intragraft myeloid cells present in biopsy-proven IRI− and IRI+ liver transplants.

Methods: RNA-sequencing was performed on 80 pre-reperfusion and post-reperfusion biopsies from 40 human recipients of liver transplantation (23 IRI+, 17 IRI−). We used transcriptional profiling and computational approaches to identify specific gene coexpression network modules correlated with functional subsets of MPO+, lysozyme+, and CD68$^+$ myeloid cells quantified by immunohistochemistry on sequential sections from the same patient biopsies.

Results: A global molecular map showed gene signatures related to myeloid activation in all patients regardless of IRI status; however, myeloid cell subsets differed dramatically in their spatial morphology and associated gene signatures. IRI− recipients were found to have a natural corticosteroid production and response profile from pre-reperfusion to post-reperfusion, particularly among monocytes/macrophages. The pre-reperfusion signature of IRI+ recipients included acute inflammatory responses in neutrophils and increased translation of adaptive

Abbreviations: DAMP, damage-associated molecular pattern; DEGs, differentially expressed genes; GO, Gene Ontology; IHC, immunohistochemistry; IRI, ischemia-reperfusion injury; LYSO, lysozyme; MPO, myeloperoxidase; TPCL, Translational Pathology Core Laboratory; UCLA, University of California, Los Angeles.

Rebecca A. Sosa and Richard Ahn contributed equally to this work.

Supplemental Digital Content is available for this article. Direct URL citations are provided in the HTML and PDF versions of this article on the journal's website, www.hepcommjournal.com.

immune-related genes in monocytes/macrophages coupled with decreased glucocorticoid responses. Subsequent lymphocyte activation at post-reperfusion identified transcriptional programs associated with the transition to adaptive immunity found only among IRI+ recipients.

Conclusions: Myeloid subset-specific genes and related signaling pathways provide targets for the development of therapeutic strategies aimed at limiting IRI in the clinical setting of liver transplantation.

INTRODUCTION

Liver ischemia-reperfusion injury (IRI) is an acute inflammatory condition that can affect patients after OLT and significantly contributes to early allograft dysfunction and post-transplant rejection.[1] Animal models and human transplant studies show that liver IRI is caused by ischemia-induced hypoxia during the procurement and preservation of the donor liver and reperfusion-induced inflammation during transplantation. Together, these states induce cellular stress and apoptosis that can lead to immune activation of tissue-resident macrophages (KCs) and infiltrating recipient immune cells, most notably myeloid cells.[1–5] Transcriptomics of human livers undergoing warm or cold ischemia, either alone or with reperfusion has been explored.[6–9] However, these studies did not evaluate biopsy-proven IRI, which can be assessed at a 2-hour reperfusion.[10,11] To address this lack of understanding regarding the transcriptomics of OLT-IRI, we performed the first RNA-sequencing study of liver biopsy samples that were histologically graded pre-reperfusion and post-reperfusion using our published IRI scoring system. In this study, we describe genes differentially expressed in IRI+ versus IRI− OLT recipients at either pre-reperfusion or post-reperfusion. We quantified functional myeloid subsets using immunohistochemistry (IHC) for cells with primarily innate immune system functions [myeloperoxidase (MPO)+ neutrophils], phagocytic cells capable of antigen presentation and activation of an adaptive immune response ($CD68^+$), or multipotential for activating as either population [lysozyme (LYSO)+ myeloid cells]. Further, we identified weighted gene coexpression network modules that correlate with resident and/or infiltrating myeloid populations, which likely play a role in either augmenting or suppressing the development of IRI. Identifying this transcriptomic signature of liver IRI sets the stage for a better understanding of the processes that underlie this injury and could provide molecular targets for potential therapeutics aiming to decrease the incidence of IRI in future recipients of OLT.

METHODS

Patient recruitment and sample collection

Adult recipients of OLT were recruited at UCLA, and routine standard-of-care and immunosuppressive therapy were administered, as specified by UCLA liver transplant protocols. Study data were collected and managed using REDCap.[12] All studies described were reviewed and approved by the UCLA Institutional Research Board (IRB; #13-000143). Patients gave written informed consent before their participation in the study. Donor organs were obtained from brain death and circulatory death donors with standardized techniques. No donor organs were obtained from executed prisoners or other institutionalized persons. The donor livers were perfused with and stored in cold University of Wisconsin solution (ViaSpan; Bristol-Meyers Squibb Pharma). Cold ischemia time was defined as the time from perfusion of the donor liver with University of Wisconsin solution to the removal of the liver from cold storage. Needle biopsies were taken from the left lobe 2 hours before reperfusion and after complete revascularization of the liver 2 hours after reperfusion. Biopsy samples were divided into 2 halves, with one half formalin-fixed and paraffin embedded for IHC studies and the other half stored in RNAlater for RNA-sequencing.

Liver histopathological IRI scoring

Biopsy scoring for IRI was done as described.[10] Briefly, formalin-fixed, paraffin-embedded pre-reperfusion and post-reperfusion biopsies were stained with hematoxylin and eosin, following a standardized protocol by the Translational Pathology Core Laboratory (TPCL) at UCLA. Stained post-reperfusion biopsies were reviewed by a single transplant hepatopathologist and scored for necrosis and inflammation on a continuum of IRI severity. Recipients of liver transplantation with IRI scores of 0 to 1 are grouped as IRI−, and recipients with IRI scores of 2 to 4 are grouped as IRI+.

Myeloid cell quantification in allograft biopsies

For IHC staining, formalin-fixed, paraffin-embedded biopsy sections were stained with primary antibody to MPO, LYSO, or CD68, detected using Horseradish Peroxidase (Agilent), visualized with 3, 3-diaminobenzadine, and counterstained with hematoxylin. Whole stained slides were converted to high-resolution digital bright-field images using an Aperio ScanScope AT high throughput scanning system with up to ×40 (0.75 NA, 0.23 μm/pixels; Leica Biosystems).

Slides were viewed in Aperio ImageScope software (Leica Biosystems), and regions of interest were drawn around areas containing relevant, good-quality, biopsy tissue with at least 4 portal tracts. Images with ROIs were then quantified for positively stained myeloid cells using object-based analysis in Tissue Studio (Definiens AG, Munchen, Germany).

Tissue areas were identified by Tissue Studio using automatic thresholding for homogeneity, brightness, and minimal tissue size. Tissue Studio was trained to recognize cells positively stained for MPO+, LYSO+, or $CD68^+$ using the cellular analysis feature on 4 digital slides of positive control tissues for each marker. Nucleus detection was performed by defining hematoxylin and IHC intensity thresholds, and nucleus morphology was filtered using area, roundness, and width measurements. Cell simulation was defined in Tissue Studio by maximum cell growth (μm from nucleus). This strategy was then applied to patient biopsy samples. Data obtained from the resulting image objects (segments) for each virtual slide were exported as tables in Excel (Microsoft), including counts of the number of positively stained cells, total cell number, and the absolute area of the tissue/predefined ROI. Data were then normalized as positive cell number per millimeter of tissue squared ($\#/mm^2$).

RNA sample preparation and sequencing

RNA was isolated from needle core biopsies obtained 2 hours pre-reperfusion or post-reperfusion and stored in RNAlater. Libraries were prepared for samples that passed quality control using the KAPA-stranded mRNA kit (https://sequencing.roche.com). Single-read sequencing with a read length of 50 bp was performed using the Illumina HiSeq3000 platform by the Technology for Genomics and Bioinformatics facility at UCLA.

Read quality control and alignment

Quality control of reads was checked using FastQC 0.11.8. Reads were aligned to the GRCh38 human reference genome using STAR 2.5.1b.[13] Indexing of the BAM files and removal of PCR duplicates was performed using samtools[14] and picard (https://github.com/broadinstitute/picard). The final counts table used for downstream analyses was produced using featureCounts.[15]Transcript abundances are expressed as transcripts per million log2 scale. Data have been deposited in the National Center for Biotechnology Information's Gene Expression Omnibus (GEO) and are accessible through GEO series accession number GSE151648.

Differential expression analysis and pathway analysis

Using edgeR 3.9 package in R we converted the raw counts to counts-per-million, performed normalization, and tested for differential expression[16] between (1) IRI+ and IRI− at the pre-reperfusion timepoint, (2) IRI+ and IRI− at the post-reperfusion timepoint, and (3) between pre-reperfusion and post-reperfusion timepoints for IRI− or IRI+ samples separately. We used gProfiler to perform canonical pathway enrichment analysis of the differentially expressed genes (DEGs).[17]

Weighted gene coexpression network analysis and correlation with cell counts

We performed quality control on the matrix of normalized expression values to remove any transcripts with either zero variance or a missing value prior to implementing weighted gene coexpression network analysis in R.[18] We created the weighted adjacency matrix with a soft thresholding parameter, β, for the power function set to 12 and used it to generate a topological overlap matrix and dendrogram that was pruned using a dynamic hybrid branch cutting method with a cut height of 0.3 to merge module eigengenes (the first principal component of each network) so that modules with a correlation of 0.7 or greater were merged (minimum size of a module is set at 30 genes). MEs were calculated by performing a singular value decomposition on the topological overlap matrix. We defined module membership, MM, as the absolute correlation between each gene in a network module and its module eigengenes. Finally, we correlated the cell counts of MPO+-stained, LYSO+-stained, and $CD68^+$-stained cells with MEs.

Statistical analysis

To test for association between demographic data and IRI status, Fisher exact was implemented for categorical variables while Student *t* test was implemented for

continuous variables. Hierarchical clustering was performed on columns using the Euclidean distance for the column distance measure and Ward D for the clustering method. All statistical analyses were performed in R.

RESULTS

Demographic and clinical data

Demographic and clinical features of recipients of OLT (n = 40) and their donors are shown in Table 1. Biopsies of donor allografts obtained 2 hours pre-reperfusion, and post-reperfusion were scored by histopathology for inflammation and necrosis as previously described. There was no significant association between recipient, donor, or transplant clinical or demographic characteristics and IRI status (Table 1).

IRI has a unique pretransplant transcriptomic profile

To identify genes that are differentially expressed between pre-reperfusion biopsy samples from IRI+ (n = 23) and IRI− (n = 17) recipients of OLT, we performed RNA-sequencing on biopsies obtained 2 hours before reperfusion. There were 65 DEGs between IRI ± at the pre-reperfusion timepoint, with 60 upregulated and 5 downregulated in IRI+ versus IRI− patients (False Discovery Rate ≤ 0.1) (Figure 1A; Supplemental Table S1, http://links.lww.com/HC9/A727). Upregulated DEGs included pattern recognition receptor genes (*CLEC4D*, *FPR1*, *FPR2*, and *TREM1*), damage-associated molecular pattern (DAMP) genes (*HSPA6*, *S100A8*, *S100A9*, and *S100A12*), the inflammation-associated enzyme Cyclooxygenase-2 (*PTGS2*), and genes involved in neutrophil recruitment (*CXCL8*, *CXCR1*, *CXCR2*, *FCN1*, *HSPA6*, *TNFAIP6*, and *CLEC4D*). An unsupervised heatmap of these 65 pre-reperfusion DEGs predominantly clustered recipients of OLT by their IRI status (Figure 1B), with the IRI+ cluster being 77% IRI+ (17/22) and the IRI− cluster being 69% IRI− (11/16). Pathway enrichment analysis of the 65 DEGs revealed that the top significantly enriched pathways included neutrophil activation, innate immune system, DAMP receptor binding, and cytokine-cytokine receptor interaction (p-value < 0.05) (Figure 1C; Supplemental Table S2, http://links.lww.com/HC9/A728).

IRI alters the post-transplant transcriptomic profile

Testing for differential expression between the pre-transplant and post-transplant timepoints (PRE vs. POST) in stratified analyses of IRI− samples or IRI+ samples separately, we observed that 573 genes were differentially expressed in both IRI− and IRI+ samples (540 upregulated, 33 downregulated) ($\log_2$-Fold Change ≥ 1, False Discovery Rate < 0.1), 330 genes were exclusively differentially expressed in the IRI+ samples (247 genes upregulated, 83 downregulated), and 202 genes were exclusively differentially expressed in the IRI− samples (155 genes upregulated, 47 downregulated; Figure 2; Supplemental Table S3, http://links.lww.com/HC9/A729). Top pathways enriched for with DEGs exclusively in the IRI− samples included hemoglobin biosynthetic process, IL-8 receptor activity, ROS metabolic process, response to hypoxia, and response to organic cyclic compound (Figure 2; Supplemental Table S4, http://links.lww.com/HC9/A730). Top pathways that were significantly enriched with DEGs exclusively in the IRI + samples included innate immune response, leukocyte activation, IL-4 and IL-13 signaling, and neutrophil activation. These transcriptomic profiles reveal how the reperfusion maneuver specifically differs in IRI− and IRI+ patients and which specific biological processes directly associated with either a “low-risk” IRI− or a “high-risk” IRI+ endotype.

Specific myeloid cell populations correlate with different weighted gene coexpression network modules in IRI− and IRI+ patients who underwent OLT

We previously reported the importance of myeloid cells in IRI, particularly in regard to DAMP/pattern recognition receptor signaling.[19] Therefore, we next focused our analysis on the impact of myeloid cell populations present in the biopsies on the transcriptomic signatures of the allografts. First, we identified specific myeloid genotypes on a continuum of gene expression of *MPO*, *LYSO*, or *CD68*. We then stained adjacent tissue sections for lineage-associated markers commonly used in the clinical setting: MPO (primarily neutrophils), lysozyme (LYSO; pan-myeloid cells), or CD68 (activated phagocytic monocytes/macrophages, including tissue-resident KCs). The number of MPO+ (Figure 3A), LYSO+ (Figure 3B), or $CD68^+$ (Figure 3C) cells was quantified in IRI+ versus IRI− patient biopsy samples, and the cell counts were used to identify groups of patients with myeloid cell counts above the median as having phenotypes of MPO^{hi}, $LYSO^{hi}$, or $CD68^{hi}$. Myeloid genotypes and phenotypes were correlated with networks of coexpressed genes using weighted gene coexpression analysis WCGNA, which identifies biologically meaningful networks of coexpressed genes in an unsupervised fashion (Figure 3D). We identified 26 network modules using weighted gene coexpression network analysis, 22 of which were significantly

TABLE 1 Clinical and demographic data

Clinical and demographic data Characteristic	ALL (n = 40)	IRI− (n = 17)	IRI+ (n = 23)	p[a]
Recipient				
Age, years (mean ± SD)	54 ± 11	52 ± 12	55 ± 10	0.44
Sex [n (%)]	—	—	—	0.34
Female	17 (43)	9 (53)	8 (35)	—
Male	23 (58)	8 (47)	15 (65)	—
Race [n (%)]	—	—	—	0.19
Asian	4 (10)	2 (12)	2 (9)	—
Black/African American	3 (8)	3 (18)	0	—
White/Caucasian	23 (58)	8 (47)	15 (65)	—
Other/unknown	10 (25)	4 (24)	6 (26)	—
Ethnicity [n (%)]	—	—	—	0.39
Hispanic/Latino	18 (45)	9 (53)	9 (39)	—
Non-Hispanic/Latino	22 (55)	8 (47)	14 (61)	—
Liver disease etiology [n (%)]	—	—	—	0.18
Alcohol-associated	20 (50)	6 (36)	14 (61)	—
HBV	5 (13)	3 (18)	2 (9)	—
HCV	6 (15)	2 (12)	4 (17)	—
NASH	6 (15)	5 (29)	1 (4)	—
Other	3 (8)	1 (6)	2 (9)	—
HCC [n (%)]	5 (13)	2 (12)	3 (13)	> 0.99
MELD, at list [mean ± SD]	33 ± 10	33 ± 10	32 ± 9	0.07
MELD, at transplant [mean ± SD]	38 ± 4	38 ± 4	38 ± 4	> 0.99
Transplant(s) [n (%)]	—	—	—	0.08
Isolated liver	36 (90)	16 (94)	20 (87)	—
Liver-kidney	4 (10)	1 (6)	3 (13)	—
Donor				
Age, y [mean ± SD]	36 ± 13	34 ± 13	37 ± 14	0.51
Sex [n (%)]	—	—	—	0.20
Female	16 (33)	9 (56)	7 (44)	—
Male	24 (68)	8 (33)	16 (67)	—
Race [n (%)]	—	—	—	0.41
Asian	3 (8)	0	3 (13)	—
Black/African American	5 (13)	3 (18)	2 (9)	—
White/Caucasian	20 (50)	9 (53)	11 (48)	—
Other/undisclosed	12 (30)	5 (29)	7 (44)	—
Ethnicity [n (%)]	—	—	—	0.82
Hispanic/Latino	11 (28)	5 (29)	6 (26)	—
Non-Hispanic/Latino	29 (72)	12 (71)	17 (74)	—
Status [n (%)]	—	—	—	> 0.99
DBD	38 (95)	16 (94)	22 (96)	—
DCD	2 (5)	1 (6)	1 (4)	—
Warm ischemia, min [mean ± SD]	52 ± 17	50 ± 14	54 ± 21	0.57
Cold ischemia, h [mean ± SD]	7 ± 2	7 ± 1	8 ± 2	0.12
Recipient + donor				
ABO [n (%)]	—	—	—	0.74
Identical	149 (91)	118 (90)	31 (94)	—
Compatible	15 (9)	13 (10)	2 (6)	—
DRI [mean ± SD]	1.4 ± 0.3	1.4 ± 0.4	1.3 ± 0.3	0.23

[a] *t* test for continuous variables; Fisher exact test for categorical variables.

Abbreviations: DBD, Donation after Brain Death; DCD, Donation after Circulatory Death; DRI, Donor Risk Index; IRI, ischemia-reperfusion injury; MELD, Model for End-Stage Liver Disease.

correlated with *MPO*, *LYSO*, or *CD68* copy numbers or MPO^{hi}, LYSO^{hi}, or CD68^{hi} (Figure 3D; Supplemental Tables S5–S30, S5 http://links.lww.com/HC9/A731, S6 http://links.lww.com/HC9/A732, S7 http://links.lww.com/HC9/A733, S8 http://links.lww.com/HC9/A734, S9 http://links.lww.com/HC9/A735, S10 http://links.lww.com/HC9/A736, S11 http://links.lww.com/HC9/A737, S12 http://links.lww.com/HC9/A738, S13 http://links.lww.com/HC9/A739, S14 http://links.lww.com/HC9/A740, S15 http://links.lww.com/HC9/A741, S16 http://links.lww.com/HC9/A742, S17 http://links.lww.com/HC9/A743, S18 http://links.lww.com/HC9/A744, S19 http://links.lww.com/HC9/A745, S20 http://links.lww.com/HC9/A746, S21 http://links.lww.com/HC9/A747, S22 http://links.lww.com/HC9/A748, S23 http://links.lww.com/HC9/A749, S24 http://links.lww.com/HC9/A750, S25 http://links.lww.com/HC9/A751, S26 http://links.lww.com/HC9/A752, S27 http://links.lww.com/HC9/A753, S28 http://links.lww.com/HC9/A754, S29 http://links.lww.com/HC9/A755, S30 http://links.lww.com/HC9/A756).

MPO+cells are associated with different gene signatures in IRI+ versus IRI− recipients of OLT

MPO is a lysosomal enzyme produced in high amounts by neutrophils, especially during their maturation phase. MPO+ cells were present within the donor allografts prior to transplantation (PRE) in similar numbers between IRI− and IRI+ individuals (507 ± 326 vs. 465 ± 280 cells per mm^2); Figure 3A). MPO+ cells were larger and more frequently in portal tract areas in IRI− patients at the PRE timepoint than MPO+ cells in IRI+ recipients, where cells remained small and diffuse (Figure 4A). MPO+ cell numbers remained similar at the POST timepoint for IRI− recipients but were significantly higher in IRI+ recipients (Figure 3A; 416 ± 237 vs. 897 ± 602 cells per mm^2). At the POST timepoint, MPO+ cells in biopsies from IRI− patients were small and diffuse, whereas MPO+ cells in IRI+ recipients were large and found in clusters (Figure 4A).

IRI− patients with a pretransplant MPO^{hi} phenotype positively correlated with ME17, which contains GO terms associated with steroid synthesis (Figures 3B, 4B; Supplemental Table S21, http://links.lww.com/HC9/A747), whereas IRI+MPO^{hi} patients positively correlated with ME18, associated with GO terms of an acute inflammatory response (Figures 3B, 4B; Supplemental Table S22, http://links.lww.com/HC9/A748), and negatively correlated with ME2, ME5, ME6, and ME16 (Figure 3B, Supplemental Tables S6 http://links.lww.com/HC9/A732, S9 http://links.lww.com/HC9/A735, S10 http://links.lww.com/HC9/A736, and S20 http://links.lww.com/HC9/A746). At the POST timepoint, there were no modules significantly associated with MPO^{hi} cell counts in IRI− patients. However, ME2, ME15, and ME24 positively associated with the MPO copy numbers, and module eigengenes 17 and ME26 negatively associated with the MPO^{hi} phenotype in IRI+ patients (Figure 3B, Supplemental Tables S6 http://links.lww.com/HC9/A732, S19 http://links.lww.com/HC9/A745, S21 http://links.lww.com/HC9/A747, S28 http://links.lww.com/HC9/A754, S30 http://links.lww.com/HC9/A756). ME2 contains terms related to increased transcription and translation, and ME24 contains terms related to immune cell activation and proinflammatory responses (Figure 4B).

LYSO+ cells are associated with different gene signatures in IRI+ versus IRI− recipients of OLT

LYSO is an antimicrobial enzyme predominantly produced by cells of the myeloid lineage, including both neutrophils and macrophages, as well as progenitors and differentiating cells. LYSO+ cells were present within the donor allografts prior to transplantation (PRE) in similar numbers between IRI− and IRI+ individuals (620 ± 235 vs. 506 ± 216 cells per mm^2; Figure 3A). LYSO+ cell numbers remained similar at the POST timepoint for IRI− recipients, but were significantly higher in IRI+ recipients (512 ± 192 vs. 923 ± 580 cells per mm^2). Similar to what was observed in MPO+ cells, LYSO+ cells were larger and more frequently in portal tract areas in IRI− patients at the PRE timepoint than LYSO+ cells in IRI+ recipients, where cells remained small and diffuse (Figure 5A). At the POST timepoint, LYSO+ cells in biopsies from IRI− patients were small and diffuse, whereas LYSO+ cells in IRI+ recipients were large and found in clusters.

Also similar to the MPO^{hi} phenotype in IRI− patients at the PRE timepoint, the LYSO^{hi} phenotype in IRI− patients at the PRE timepoint correlated with ME17 and steroid synthesis (Figures 3B, 5B; Supplemental Table S21, http://links.lww.com/HC9/A747). Pretransplant IRI+ patients with increased *LYSO* counts were positively correlated with 2 modules, ME15, ME19, and ME22 (Figure 3B, Supplemental Tables S19 http://links.lww.com/HC9/A745, S23 http://links.lww.com/HC9/A749, and S26 http://links.lww.com/HC9/A752). ME19 contains GO terms associated with immune cell migration and activation (Figure 5B; Supplemental Table S23 http://links.lww.com/HC9/A749), and ME22 contains GO terms associated with adaptive immune responses (Figure 5B; Supplemental Table S26 http://links.lww.com/HC9/A752). At the POST timepoint, *LYSO* gene counts positively correlated with ME16 in IRI− recipients, which contains GO terms associated with a response to steroids (Figure 5B; Supplemental Table S20 http://links.lww.com/HC9/A746), whereas the LYSO^{hi} IRI+ patient phenotype positively correlated with ME2, ME5, and ME7 (Figure 3B;

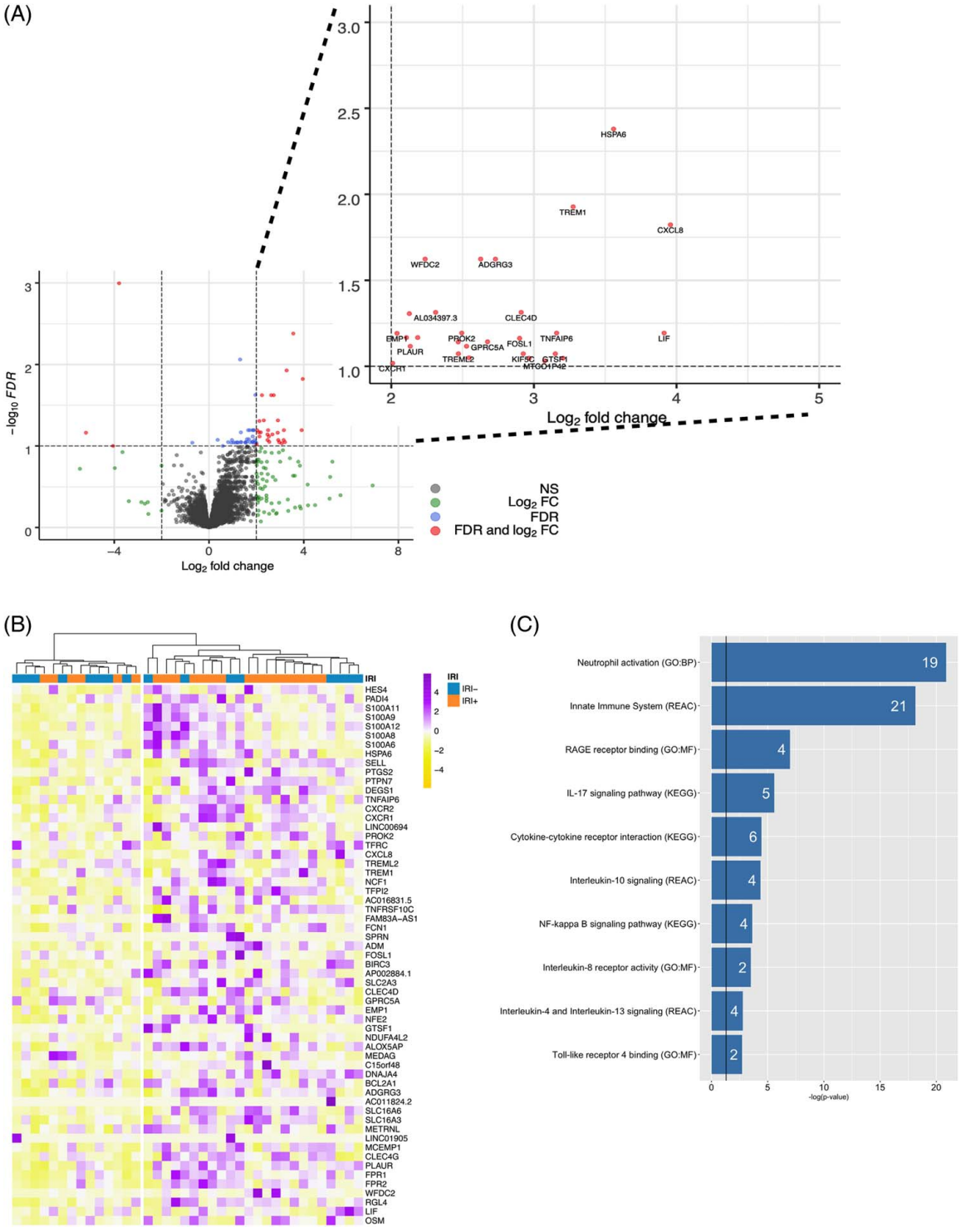

FIGURE 1 Genes are differentially expressed between IRI+ and IRI− biopsies at the pretransplant timepoint. (A) Volcano plot of genes differentially expressed between IRI+ and IRI− patient biopsies at the pretransplant timepoint, with zoomed-in view of genes differentially expressed with log2FC ≥ 4 and FDR < 0.1. (B) Heatmap of genes differentially expressed between IRI+ and IRI− patient biopsies at the pretransplant timepoint (log2FC ≥ 4, FDR < 0.1), with samples hierarchically clustered in an unsupervised manner. (C) GO, REAC, or KEGG pathways that are significantly enriched for by the genes differentially expressed between IRI+ and IRI− patient biopsies at the pretransplant timepoint. The number of genes enriched for in a pathway is indicated in the bar. Black vertical line corresponds to a *p*-value of 0.05. Abbreviations: DEG, differentially expressed gene; BP, Biological Process; FC, Fold Change; FDR, False Discovery Rate; GO, Gene Ontology; IRI, ischemia-reperfusion injury; KEGG, Kyoto Encyclopedia of Genes and Genomes; ME, Module Eigengene; REAC, reactome.

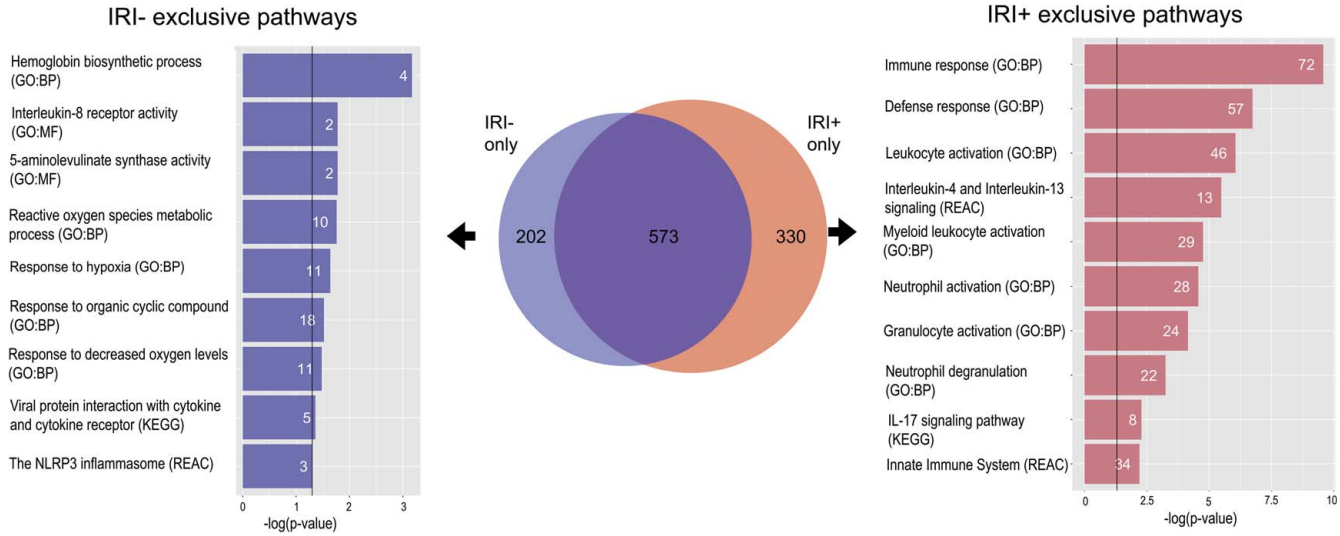

FIGURE 2 IRI+ and IRI− patients have distinct changes in their transcriptomic profiles between the pretransplant and post-transplant timepoints. Venn diagram displaying number of differentially expressed genes (log2FC ≥ 4, FDR < 0.1) between pretransplant and post-transplant that are exclusive to IRI+ samples (n = 330), exclusive to IRI− samples (n = 202), or shared between IRI ± samples (n = 573). Selected GO, Reactome (REAC), or KEGG pathways that are significantly enriched by genes that are exclusively differentially expressed between pretransplant and post-transplant timepoints for IRI+ or IRI− samples are shown. The number of genes enriching for a pathway is indicated in the bar. Black vertical line corresponds to a *p*-value of 0.05. Abbreviations: BP, Biological Process; FC, Fold Change; FDR, False Discovery Rate; GO, Gene Ontology; IRI, ischemia-reperfusion injury; KEGG, Kyoto Encyclopedia of Genes and Genomes; MF, Molecular Function; REAC, reactome.

Supplemental Tables S6 http://links.lww.com/HC9/A732, S9 http://links.lww.com/HC9/A735, and S11 http://links.lww.com/HC9/A737), and negatively correlated with ME4, ME22 and ME26 (Figure 3B; Supplemental Tables S8 http://links.lww.com/HC9/A734, S26 http://links.lww.com/HC9/A752, and S30 http://links.lww.com/HC9/A756). The *LYSO* genotype for post-IRI+ also correlates with ME2 and ME5 and negatively correlates with ME26. ME7 contains GO terms related to protein translation (Figure 5B, Supplemental Table S11, http://links.lww.com/HC9/A737).

CD68^{+} cells are associated with different gene signatures in IRI+ versus IRI− recipients of OLT

CD68 is an intracellular glycoprotein primarily associated with cytoplasmic granules under homeostatic conditions that cycle to the cell membrane in phagocytic macrophages. Tissue-resident macrophages such as KCs express CD68 in high amounts, as do actively phagocytosing infiltrating myeloid cells. CD68^{+} cells were present within the donor allografts prior to transplantation (PRE) in similar numbers between IRI− and IRI+ individuals (323 ± 203 vs. 295 ± 204 cells per mm^2; Figure 3A). Similar numbers of CD68^{+} cells were seen at the POST timepoint for IRI+/− recipients as their baseline numbers (257 ± 211 vs. 292 ± 169 cells per mm^2); however, very large CD68+cells can be seen in the POST biopsies from IRI+ recipients as compared with other settings (Figure 6A).

The CD68^{hi} phenotype in IRI− patients at the PRE timepoint positively correlated with ME3 and negatively correlated with ME5, ME6, ME9, ME10, ME18, and ME26 (Figures. 3B, 6B; Supplemental Tables S7, http://links.lww.com/HC9/A733, S9, http://links.lww.com/HC9/A735, S10, http://links.lww.com/HC9/A736, S13, http://links.lww.com/HC9/A739, and S22, http://links.lww.com/HC9/A748). CD68 genotype correlations were also negative for ME18 and positive for ME24. ME3 contains GO terms associated with metabolism and catabolism (Figure 6B, Supplemental Table S7, http://links.lww.com/HC9/A733), whereas ME9 is associated with protein translation and trafficking (Figure 6B, Supplemental Table S13, http://links.lww.com/HC9/A739). CD68^{hi} cell counts positively correlated with ME1, ME7, ME13, ME15, ME18, and ME26 (Figure 3B; Supplemental Tables S5, http://links.lww.com/HC9/A731, S11, http://links.lww.com/HC9/A737, S17, http://links.lww.com/HC9/A743, S18, http://links.lww.com/HC9/A744, S19, http://links.lww.com/HC9/A745, S22, http://links.lww.com/HC9/A748, and S30, http://links.lww.com/HC9/A756), and negatively correlated with ME2, ME5, ME6, ME12, and ME16 at the PRE timepoint in IRI+ recipients (Figure 3B; Supplemental Tables S6, http://links.lww.com/HC9/A732, S9, http://links.lww.com/HC9/A735, S10, http://links.lww.com/HC9/A736, S16, http://links.lww.com/HC9/A742, and S20, http://links.lww.com/HC9/A746). ME13 is associated with immune cell activation (Figures 3B, 6B; Supplemental Table S17, http://links.lww.com/HC9/A743). CD68 gene counts positively correlated with ME13, ME14, ME18,

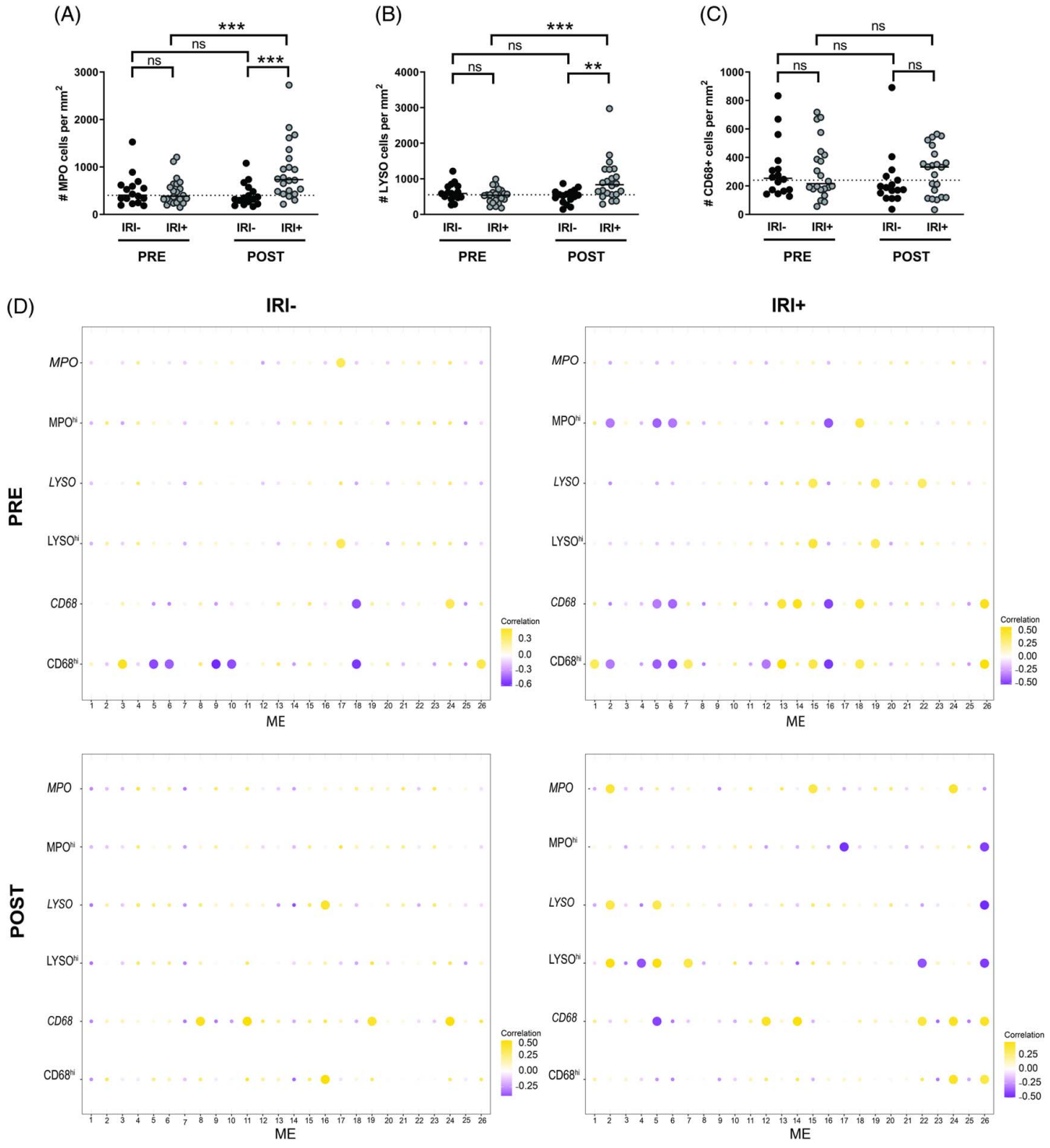

FIGURE 3 Weighted gene coexpression analysis correlations with myeloid-lineage cell counts. The number of cells positive for (A) MPO, (B) LYSO, or (C) CD68 per mm^2 of tissue in pre-reperfusion or post-reperfusion biopsies. (D) Matrix plots showing the association of *MPO*, *LYSO*, and *CD68* copy numbers and MPO^{hi}, LYSO^{hi}, and CD68^{hi} phenotypes with each of the 26 module eigengenes for PRE IRI−, PRE IRI+, POST IRI− , and POST IRI+ samples. The direction and strength of the correlation are indicated by color, with yellow indicating positive correlations and purple indicating negative correlations. Small circles indicate a nonsignificant correlation, while large circles indicate a significant correlation ($p < 0.1$). Abbreviations: IRI, ischemia-reperfusion injury; LYSO, lysozyme; ME, Module Eigengene; MPO, myeloperoxidase; ns, no significance.

and ME26 and negatively correlated with ME5, ME6, and ME16. At the POST timepoint, the *CD68* genotype positively correlated with ME8, ME11, ME19, and ME24 in IRI− recipients, with the CD68^{hi} phenotype positively correlating with ME16 (Figure 3B; Supplemental Tables S12, http://links.lww.com/HC9/A738, S15, http://links.lww.com/HC9/A741, S20, http://links.lww.com/HC9/A746, S23, http://links.lww.com/

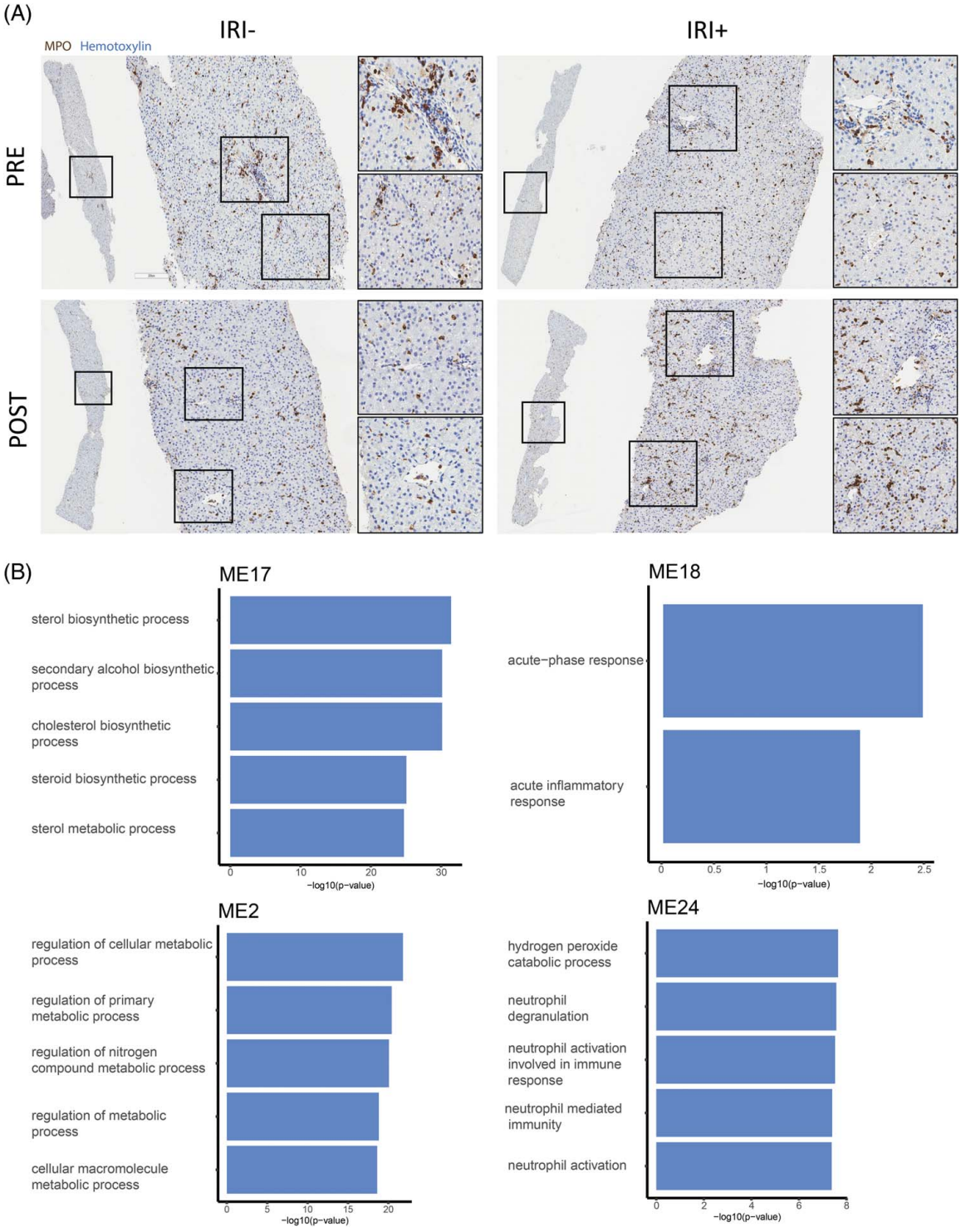

FIGURE 4 Gene modules associated with MPO+ cells in IRI− patients differ from MPO-associated gene modules in IRI+ patients. (A) Biopsies obtained from donor allografts at 2 hours pre- (PRE) or post-reperfusion (POST) were stained with MPO (brown) and counterstained with hematoxylin (blue). (B) Top 5 GO biological pathway terms that are significantly enriched with genes from ME17, ME18, ME2, and ME24. The threshold for significant enrichment was $p < 0.05$. Abbreviations: GO, Gene Ontology; ME, Module Eigengene; IRI, ischemia-reperfusion injury; MPO, myeloperoxidase.

HC9/A749, and S28, http://links.lww.com/HC9/A754). ME11 contains GO terms related to cellular adhesion (Figure 6B, Supplemental Table S15, http://links.lww.com/HC9/A741). *CD68* gene counts positively correlated with ME12, ME14, ME22, and ME26 and negatively correlated with ME5 at the POST timepoint, whereas CD68^{hi} IRI+ patients positively correlated with ME24 and ME26 (Figure 3B; Supplemental

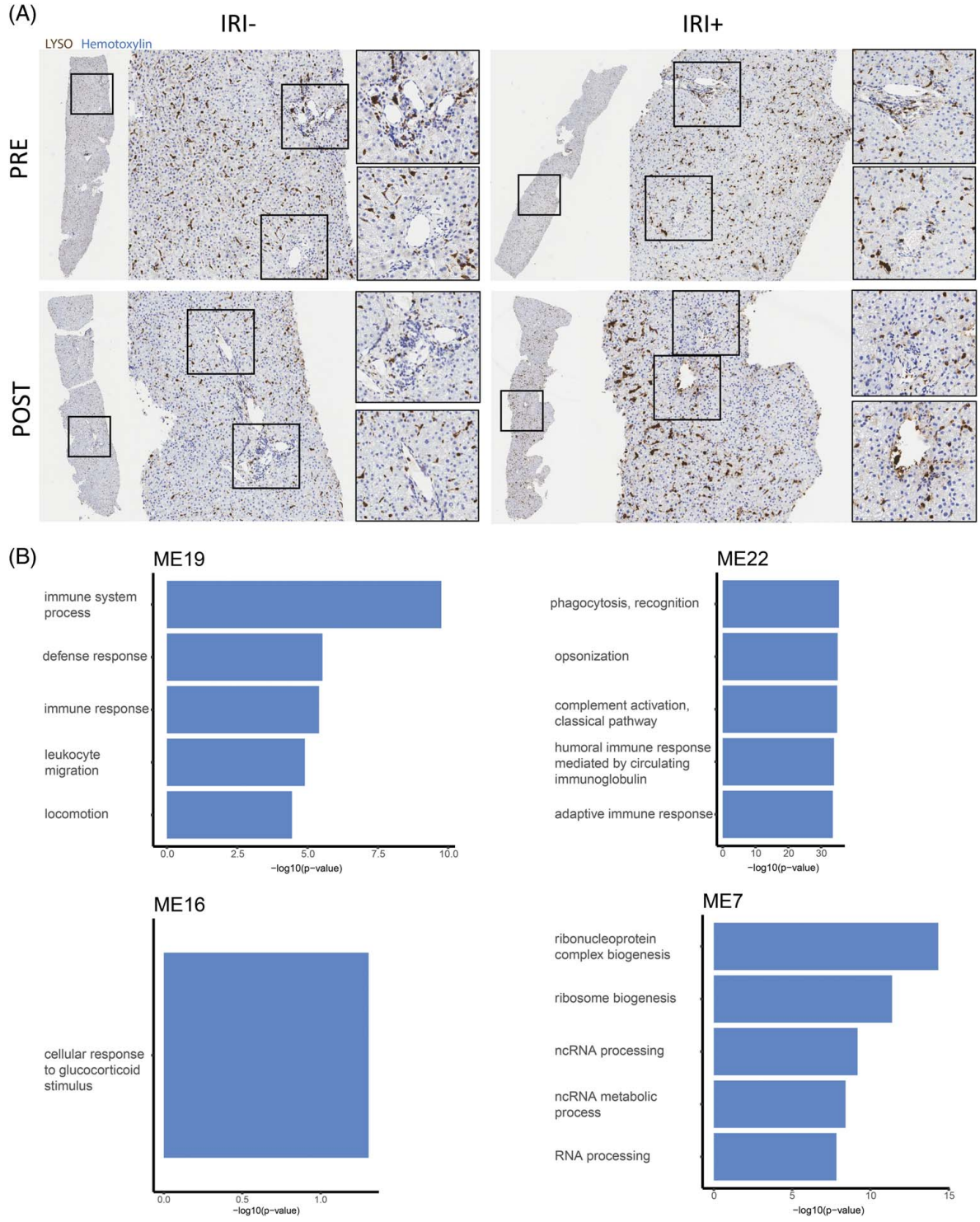

FIGURE 5 Gene modules associated with lysozyme+ cells in IRI− patients differ from lysozyme-associated gene modules in IRI+ patients. (A) Biopsies obtained from donor allografts at 2 hours pre- (PRE) or post-reperfusion (POST) were stained with lysozyme (brown) and counterstained with hematoxylin (blue). (B) Top 5 GO biological pathway terms that are significantly enriched for with genes from ME19, ME16 (only one pathway term was significantly enriched for), ME7, and ME22. The threshold for significant enrichment was $p < 0.05$. Abbreviations: GO, Gene Ontology; IRI, ischemia-reperfusion injury; ME, Module Eigengene; ncRNA, non-coding RNA.

Tables S16, http://links.lww.com/HC9/A742, S18, http://links.lww.com/HC9/A744, S26, http://links.lww.com/HC9/A752, S28, http://links.lww.com/HC9/A754, and S30, http://links.lww.com/HC9/A756).

DISCUSSION

In this study, we performed spatial phenotyping and transcriptomic analysis to reveal how immune cells

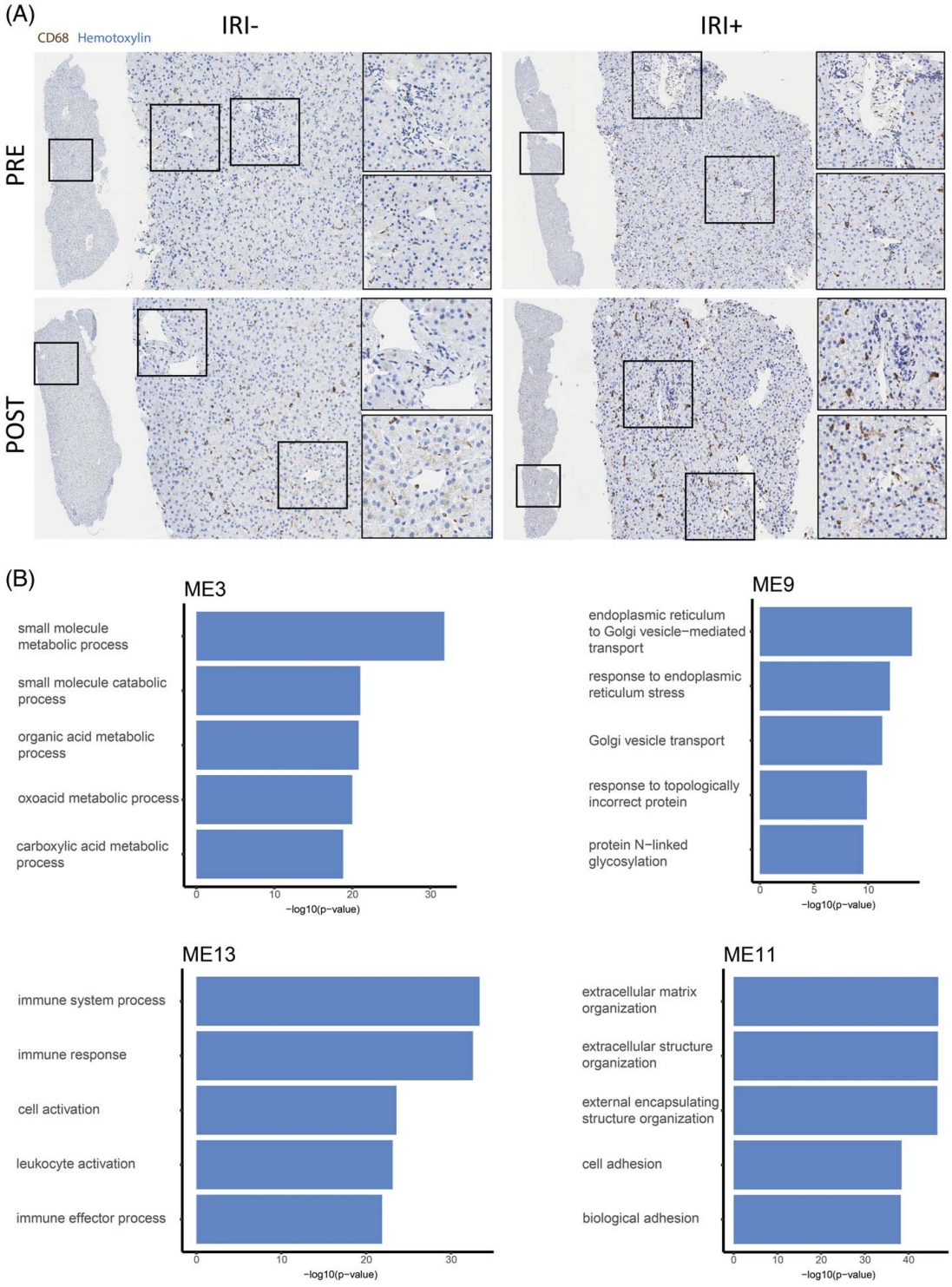

FIGURE 6 Gene modules associated with CD68$^+$ cells in IRI− patients differ from CD68-associated gene modules in IRI+ patients. (A) Biopsies obtained from donor allografts at 2 hours pre- (PRE) or post-reperfusion (POST) were stained with CD68 (brown) and counterstained with hematoxylin (blue). (B) Top 5 GO biological pathway terms that are significantly enriched with genes from ME3, ME9, ME13, and ME11. The threshold for significant enrichment was $p < 0.05$. Abbreviations: GO, Gene Ontology; IRI, ischemia-reperfusion injury; ME, Module Eigengene.

organize in the tissue landscape of IRI in patients who underwent OLT. We first characterized DEGs for IRI− and IRI+ patients at the pre-reperfusion and post-reperfusion timepoints and found that many were associated with myeloid cell activation and related immune functions. To investigate the myeloid contribution more specifically, we identified patient samples with increased numbers of 3 overlapping functional subsets of myeloid cells by MPO, LYSO, and CD68 gene and protein expression. We then created an

unsupervised coexpression network of genes using weighted gene coexpression analysis and identified subnetworks (modules) that are significantly associated with myeloid-specific genotypes and/or phenotypes. These modules were significantly enriched for pathways involved in cellular metabolism, steroid synthesis, innate immune response, and adaptive immune response but differed dramatically in association with different myeloid cell types, pre-reperfusion versus post-reperfusion timepoints, and between IRI+/− recipients of OLT. Identifying the distinct cellular and molecular phenotypes in liver IRI provides a better understanding of the processes that underlie this injury, as well as specific therapeutic targets for potential strategies to decrease the incidence of IRI in future recipients of OLT.

Analysis of pre-reperfusion biopsies revealed that unsupervised clustering correctly grouped about 70% of patients based on post-reperfusion IRI status (IRI+or IRI−), suggesting ischemic insult or protection to the allograft can be detectable at a transcriptomic level and is highly detrimental to organ quality independent from the reperfusion event. Knowing this impact of ischemia on donor livers supports current efforts to implement normothermic perfusion during graft recovery and preservation.[20] Genes upregulated in IRI+ versus IRI− pre-reperfusion biopsies included multiple inflammation-associated genes, such as pattern recognition receptors, DAMPs, and molecules involved in myeloid recruitment, that all align with signaling pathways and cell populations we and others previously confirmed to be correlated with IRI positivity.[10,19,21,22] At the post-reperfusion timepoint, pathways were exclusively associated with either IRI− or IRI+ endotypes. Although proinflammatory activation dominated the signature for IRI+ recipients, IRI− exclusive pathways included metabolic and immune responses known to participate in myeloid-mediated resilience against and/or resolution of inflammatory responses.

MPO is an antibacterial enzyme produced in high amounts by neutrophils during their maturation. Neutrophils are known to play a considerable role in IRI, arriving in large numbers to reperfuse allografts and conducting canonical innate immune response activities.[1,10] Neutrophils have been shown to form clusters at sites of injury as a result of coordinated swarming during both sterile and nonsterile inflammatory events.[23–27] These clusters then respond to local signals once they have arrived at the injury site. Neutropenia is also reported to be protective against IRI.[28] We saw a significant increase in the number of MPO+ cells present in post-reperfusion biopsies from IRI+ recipients, with significant clustering and cellular hyperplasia, suggesting their activation toward a detrimental proinflammatory phenotype. Further supporting this role, gene signatures correlated with MPO^{hi} cells in IRI+ recipients involved pathways associated with increased metabolism, transcription, translation, and proinflammatory activation. MPO+ cells in pretransplant biopsies differed dramatically in their associated gene signatures, morphology, and localization. MPO+ cells from IRI− recipients had significantly increased natural steroid synthesis, whereas a decrease in steroid response genes and an increase in acute inflammatory response genes were seen associated with MPO^{hi} cells in pretransplant biopsies from IRI+ patients. This indicates that deceased donor organs differentially respond to ischemic stress by recruiting neutrophils that provide either resilience to injury in the case of IRI− recipients or promote acute inflammation in the case of IRI+ recipients. These genes and their related pathways should be considered direct targets during normothermic perfusion therapies. For example, leveraging cholesterol synthesis as a possible intervention for limiting neutrophil skewing toward pathogenic phenotypes could be beneficial. The weighted gene coexpression analysis module ME17 is positively associated with the neutrophil signature (MPO+) in IRI− pretransplant and negatively correlated with MPO+ in IRI+ posttransplant, and it is enriched for pathways related to cholesterol biosynthesis. Further, ME18 is positively associated with MPO+ in IRI+ pretransplant and is enriched for complement-related pathways. Cholesterol is a major structural component of neutrophil plasma membranes and influences cell adhesion, a key step in transmigration.[29] Neutrophils with low cholesterol content were associated with increased inflammation in patients with cystic fibrosis.[30] Cholesterol depletion in human neutrophil cell membranes induced a more proinflammatory phenotype that included priming, enhanced activation, increased adhesion, and oxidant production.[31] The possible impact of cholesterol therapy on infectious diseases has been suggested.[32–37] Since many of the same molecular mechanisms are in play during infection as sterile inflammation, it is possible cholesterol or similar treatment during liver IRI could be a beneficial therapy for reducing infiltrating neutrophils and limiting further tissue damage and immune activation.

LYSO is an enzyme with antimicrobial properties largely produced by cells of the myeloid lineage. In the liver, strongly stained LYSO+ cells largely represent a population of highly plastic cells, which are capable of differentiating into functional immune subsets once receiving specific signals at their destination. IRI− allografts typically contained larger cells spread across all areas in the pre-reperfusion setting that became reduced in size and number after reperfusion. Genes associated with LYSO^{hi} cells in IRI− patients were similar to MPO^{hi} cells at the pre-reperfusion timepoint, with increased steroid synthesis that quickly transitioned to increased steroid response following reperfusion, indicating these cells are responding to tissue damage with a natural steroid response, providing resilience against IRI. However, IRI+ allografts had

smaller cells at the portal tracts with larger cells in other zones, particularly zone 3, where blood flow is leaving the organ, in pre-reperfusion biopsies. LYSO+ cells in IRI+ biopsies at the POST timepoint were significantly increased in number and size, with obvious colocalization at vessels with damaged endothelium, suggesting differentiation into a functional phenotype in these patients post-reperfusion. In IRI+ patients, the gene signatures significantly associated with LYSO^{hi} cells at the pre-reperfusion timepoint were related to immune cell migration and activation, including phagocytosis and adaptive immune responses. Interestingly, at the post timepoint, these adaptive immune responses were downregulated with a concomitant increase in translation machinery, with an increase in phagocytosis, supporting the idea that myeloid cells in IRI+ patients quickly differentiate into functional proinflammatory subsets by 2 hours post-reperfusion.

CD68 is a glycoprotein that becomes strongly localized to the cell membrane in phagocytic macrophages. Tissue-resident macrophages express CD68 in high amounts, as do actively phagocytosing infiltrating myeloid cells. CD68$^+$ cells in liver allografts are predominantly donor KCs in the pre-reperfusion setting and include additional infiltrating recipient cells in the post-reperfusion setting. CD68$^+$ cells were found in similar numbers in both patient groups at both timepoints. However, only the post-reperfusion biopsies from IRI+ recipients showed large, activated cells spread throughout the liver, where they were predominantly localized to damaged vessels, as has been described previously in other inflammatory states.[38,39] Gene signatures related to CD68+ cells also differed dramatically between IRI− and IRI+ patients, with IRI− CD68$^+$ cells increasing basic metabolic and catabolic pathways while downregulating protein modifications pre-reperfusion and increasing steroid response genes at the post-reperfusion timepoint. CD68$^+$ cells from IRI− patients at pre-reperfusion also increased immune cell adhesion, migration, and activation pathways, indicating they can communicate with parenchymal cells to prevent the inflammation and tissue damage seen in IRI+ allografts. In strong contrast, CD68$^+$ cells increased immune activation and translation pathways in IRI+ recipients prior to reperfusion, and upregulated adaptive immune response genes post-reperfusion. These results implicate pretransplant differences in donor KCs of IRI− or IRI+ recipients as a potential factor in the dampening or amplification of tissue damage incurred by the post-transplant allograft. Whether this is perpetuated by the same donor KCs or by infiltrating recipient myeloid cells differentiating into KCs at the post-reperfusion timepoint warrants further study so targeted therapies can be developed. In particular, this may be a way to identify individuals who may be steroid-resistant and therefore in need of more targeted therapeutic options.

We recognize the limitations of the current study, including a relatively small sample size of 40 patients. To reduce the bias associated with smaller sample sizes, we have analyzed paired biopsies from each patient to better understand the pre-reperfusion baseline and changes seen in the post-reperfusion samples. Additionally, recent advances in single-cell analysis and imaging technologies have reportedly allowed for a more in-depth comparison of the spatial and morphological phenotypes and genotypes within tissues of patients experiencing specific inflammatory disease states. However, these technologies are very expensive, with complicated data analysis and unproven clinical utility that often reduce the available sample sizes to be used even further. Therefore, we have analyzed immunohistochemical stains routinely ordered by clinicians at our center along with the highly sensitive RNAseq technique to provide the most clinically relevant information for myeloid cell subsets and related gene signatures found in human liver transplantation. Evaluation of more specialized, niche immune populations, such as dendritic cells, is outside the scope of the current study.

Overall, our data shows that IRI is associated with specific transcriptomic signatures for each myeloid cell

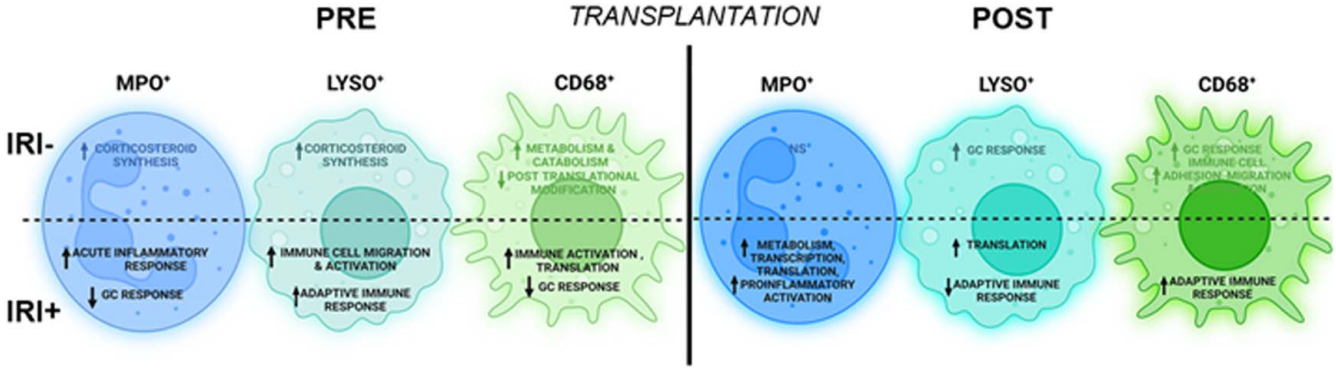

FIGURE 7 Overall transcriptomic changes in myeloid cell populations between PRE and POST timepoints for IRI− and IRI+ patients. Abbreviations: IRI, ischemia-reperfusion injury; LYSO, lysozyme; MPO, myeloperoxidase.

type at each timepoint during the transplant process (Figure 7). Genes upregulated pre-reperfusion in livers that become IRI+ have the potential to serve as markers for organ assessment during static cold storage, given that liver function tests are not available for nonperfused livers, unlike those undergoing normothermic perfusion. Genes identified as differentially expressed between pretransplant and post-transplant that are unique to IRI− and IRI+ patients, as well as gene coexpression network modules that are correlated with cell counts of $CD68^+$, LYSO+, and MPO+ cells at each of these timepoints, can serve as newly identified pathway components important in IRI manifestation. This study also provides additional targets for therapeutics—transcription factor inhibitors, siRNAs against specific transcripts, or antibodies toward proteins produced from elevated transcripts—to be developed to ultimately help clinicians improve overall long-term graft and recipient health.

DATA AVAILABILITY STATEMENT

RNA-seq data generated from this study has been deposited in the NCBI Gene Expression Omnibus repository, accession GSE151648.

AUTHOR CONTRIBUTIONS

Rebecca A. Sosa, Richard Ahn, Fang Li, David W. Gjertson, Jerzy W. Kupiec-Weglinski, Fady M. Kalda, and Elaine F. Reed designed research studies. Rebecca A. Sosa, Richard Ahn, Fang Li, Zach Qian, Bita V. Naini, and TI conducted experiments and/or acquired data. Rebecca A. Sosa, Richard Ahn, Fang Li, Allyson Q. Terry, Adil Bhat, Subha Sen, Bita V. Naini, and David W. Gjertson analyzed data. Rebecca A. Sosa, Richard Ahn, Allyson Q. Terry, and Elaine F. Reed wrote the manuscript, and Fang Li, Zach Qian, Adil Bhat, Subha Sen, Bita V. Naini, Takahiro Ito, Fady M. Kalda, Alexander Hoffmann, Ronald W. Busuttil, Jerzy W. Kupiec-Weglinski, and David W. Gjertson provided critical review of the manuscript.

FUNDING INFORMATION

NIH Ruth L. Kirschstein National Research Service Award T32CA009120 (Rebecca A. Sosa), NIH L60 MD011903 (Rebecca A. Sosa), NIH PO1 AI120944 (Jerzy W. Kupiec-Weglinski and Elaine F. Reed), and UL1TR001881 (UCLA Clinical and Translational Science Institute).

CONFLICTS OF INTEREST

Richard Ahn is employed and owns stock in Pliant. The remaining authors have no conflicts to report.

ORCID

Alexander Hoffmann https://orcid.org/0000–0002–9860–6830

REFERENCES

1. Zhai Y, Petrowsky H, Hong JC, Busuttil RW, Kupiec-Weglinski JW. Ischaemia-reperfusion injury in liver transplantation—from bench to bedside. Nat Rev Gastroenterol Hepatol. 2013;10:79–89.
2. Hirao H, Nakamura K, Kupiec-Weglinski JW. Liver ischaemia-reperfusion injury: A new understanding of the role of innate immunity. Nat Rev Gastroenterol Hepatol. 2021;19:1–18.
3. Oliveira THC, Marques PE, Proost P, Teixeira MMM. Neutrophils: A cornerstone of liver ischemia and reperfusion injury. Lab Invest. 2018;98:51–62.
4. Sun L, Wu Q, Nie Y, Cheng N, Wang R, Wang G, et al. A role for MK2 in enhancing neutrophil-derived ROS production and aggravating liver ischemia/reperfusion injury. Front Immunol. 2018;9:2610.
5. Tan Z, Jiang R, Wang X, Wang Y, Lu L, Liu Q, et al. RORgammat +IL-17+ neutrophils play a critical role in hepatic ischemia-reperfusion injury. J Mol Cell Biol. 2013;5:143–6.
6. Huang S, Ju W, Zhu Z, Han M, Sun C, Tang Y, et al. Comprehensive and combined omics analysis reveals factors of ischemia-reperfusion injury in liver transplantation. Epigenomics. 2019;11:527–42.
7. Raza A, Dikdan G, Desai KK, Shareef A, Fernandes H, Aris V, et al. Global gene expression profiles of ischemic preconditioning in deceased donor liver transplantation. Liver Transpl. 2010;16:588–99.
8. de Jonge J, Kurian S, Shaked A, Reddy KR, Hancock W, Salomon DR, et al. Unique early gene expression patterns in human adult-to-adult living donor liver grafts compared to deceased donor grafts. Am J Transplant. 2009;9:758–2.
9. Conti A, Scala S, D'Agostino P, Alimenti E, Morelli D, Andria B, et al. Wide gene expression profiling of ischemia-reperfusion injury in human liver transplantation. Liver Transpl. 2007;13:99–113.
10. Sosa RA, Zarrinpar A, Rossetti M, Lassman CR, Naini BV, Datta N, et al. Early cytokine signatures of ischemia/reperfusion injury in human orthotopic liver transplantation. JCI Insight. 2016;1:e89679.
11. Ali JM, Davies SE, Brais RJ, Randle LV, Klinck JR, Allison ME, et al. Analysis of ischemia/reperfusion injury in time-zero biopsies predicts liver allograft outcomes. Liver Transpl. 2015;21:487–99.
12. Harris PA, Taylor R, Thielke R, Payne J, Gonzalez N, Conde JG. Research electronic data capture (REDCap)—A metadata-driven methodology and workflow process for providing translational research informatics support. J Biomed Inform. 2009;42:377–81.
13. Dobin A, Davis CA, Schlesinger F, Drenkow J, Zaleski C, Jha S, et al. STAR: Ultrafast universal RNA-seq aligner. Bioinformatics. 2013;29:15–21.
14. Li H, Handsaker B, Wysoker A, Fennell T, Ruan J, Homer N, et al. The sequence alignment/map format and SAMtools. Bioinformatics. 2009;25:2078–9.
15. Liao Y, Smyth GK, Shi W. featureCounts: An efficient general purpose program for assigning sequence reads to genomic features. Bioinformatics. 2014;30:923–30.
16. Robinson MD, McCarthy DJ, Smyth GK. edgeR: A Bioconductor package for differential expression analysis of digital gene expression data. Bioinformatics. 2010;26:139–40.
17. Raudvere U, Kolberg L, Kuzmin I, Arak T, Adler P, Peterson H, et al. g:Profiler: A web server for functional enrichment analysis and conversions of gene lists (2019 update). Nucleic Acids Res. 2019;47:W191–8.
18. Langfelder P, Horvath S. WGCNA: An R package for weighted correlation network analysis. BMC Bioinformatics. 2008;9:559.
19. Sosa RA, Rossetti M, Naini BV, Groysberg VM, Kaldas FM, Busuttil RW, et al. Pattern recognition receptor-reactivity screening of liver transplant patients: Potential for personalized and precise organ matching to reduce risks of ischemia-reperfusion injury. Ann Surg. 2018. doi:10.1097/SLA.0000000000003085

20. Buchwald JE, Xu J, Bozorgzadeh A, Martins PN. Therapeutics administered during ex vivo liver machine perfusion: An overview. World J Transplant. 2020;10:1–14.
21. Sosa RA, Terry AQ, Kaldas FM, Jin YP, Rossetti M, Ito T, et al. Disulfide high-mobility group box 1 drives ischemia-reperfusion injury in human liver transplantation. Hepatology. 2020. doi:10.1002/hep.31324
22. Tian J, Avalos AM, Mao SY, Chen B, Senthil K, Wu H, et al. Toll-like receptor 9-dependent activation by DNA-containing immune complexes is mediated by HMGB1 and RAGE. Nat Immunol. 2007;8:487–96.
23. Park SA, Choe YH, Park E, Hyun YM. Real-time dynamics of neutrophil clustering in response to phototoxicity-induced cell death and tissue damage in mouse ear dermis. Cell Adh Migr. 2018;12:424–31.
24. Poplimont H, Georgantzoglou A, Boulch M, Walker HA, Coombs C, Papaleonidopoulou F, et al. Neutrophil swarming in damaged tissue is orchestrated by connexins and cooperative calcium alarm signals. Curr Biol. 2020;30:2761–76.e2767.
25. Ng LG, Qin JS, Roediger B, Wang Y, Jain R, Cavanagh LL, et al. Visualizing the neutrophil response to sterile tissue injury in mouse dermis reveals a three-phase cascade of events. J Invest Dermatol. 2011;131:2058–68.
26. Khazen R, Corre B, Garcia Z, Lemaître F, Bachellier-Bassi S, d'Enfert C, et al. Spatiotemporal dynamics of calcium signals during neutrophil cluster formation. Proc Natl Acad Sci USA. 2022;119:e2203855119.
27. Lämmermann T, Afonso PV, Angermann BR, Wang JM, Kastenmüller W, Parent CA, et al. Neutrophil swarms require LTB4 and integrins at sites of cell death in vivo. Nature. 2013;498:371–5.
28. Honda M, Takeichi T, Hashimoto S, Yoshii D, Isono K, Hayashida S, et al. Intravital imaging of neutrophil recruitment reveals the efficacy of FPR1 blockade in hepatic ischemia-reperfusion injury. J Immunol. 2017;198:1718–28.
29. Tucker B, Ephraums J, King TW, Abburi K, Rye KA, Cochran BJ. Impact of impaired cholesterol homeostasis on neutrophils in atherosclerosis. Arterioscler Thromb Vasc Biol. 2023;43:618–27.
30. White MM, Geraghty P, Hayes E, Cox S, Leitch W, Alfawaz B, et al. Neutrophil membrane cholesterol content is a key factor in cystic fibrosis lung disease. EBioMedicine. 2017;23:173–84.
31. Solomkin JS, Robinson CT, Cave CM, Ehmer B, Lentsch AB. Alterations in membrane cholesterol cause mobilization of lipid rafts from specific granules and prime human neutrophils for enhanced adherence-dependent oxidant production. Shock. 2007;28:334–8.
32. Kipp HA. Variation in the cholesterol content of the serum in pneumonia. J Biol Chem. 1920;44:215–37.
33. Song Z, Bai J, Nauwynck H, Lin L, Liu X, Yu J, et al. 25-Hydroxycholesterol provides antiviral protection against highly pathogenic porcine reproductive and respiratory syndrome virus in swine. Vet Microbiol . 2019;231:63–70.
34. Zhang Z, Datta G, Zhang Y, Miller AP, Mochon P, Chen Y-F, et al. Apolipoprotein AI mimetic peptide treatment inhibits inflammatory responses and improves survival in septic rats. Am J Physiol Heart Circ. 2009;297:H866–73.
35. Kwon WY, Suh GJ, Kim KS, Kwak YH, Kim K. 4F, apolipoprotein AI mimetic peptide, attenuates acute lung injury and improves survival in endotoxemic rats. J Trauma Acute Care Surg. 2012;72:1576–83.
36. Pajkrt D, Doran J, Koster F, Lerch P, Arnet B, Van Der Poll T, et al. Antiinflammatory effects of reconstituted high-density lipoprotein during human endotoxemia. J Exp Med. 1996;184:1601–8.
37. Dellinger RP, Tomayko JF, Angus DC, Opal S, Cupo MA, McDermott S, et al. Efficacy and safety of a phospholipid emulsion (GR270773) in Gram-negative severe sepsis: Results of a phase II multicenter, randomized, placebo-controlled, dose-finding clinical trial. Crit Care Med. 2009;37:2929–38.
38. Tomita M, Yamamoto K, Kobashi H, Ohmoto M, Tsuji T. Immunohistochemical phenotyping of liver macrophages in normal and diseased human liver. Hepatology. 1994;20:317–25.
39. McWhorter FY, Davis CT, Liu WF. Physical and mechanical regulation of macrophage phenotype and function. Cell Mol Life Sci. 2015;72:1303–6.

How to cite this article: Sosa RA, Ahn R, Li F, Terry AQ, Qian Z, Bhat A, et al. Myeloid spatial and transcriptional molecular signature of ischemia-reperfusion injury in human liver transplantation. Hepatol Commun. 2024;8:e0330. https://doi.org/10.1097/HC9.0000000000000330